Evolution of non-uniformly seeded warm clouds in idealized turbulent conditions

2008 New J. Phys. 10 075019

(http://iopscience.iop.org/1367-2630/10/7/075019)

New Journal of Physics
The open-access journal for physics

Evolution of non-uniformly seeded warm clouds in idealized turbulent conditions

Stanislav Derevyanko[1,3], **Gregory Falkovich**[2] **and Sergei Turitsyn**[1]

[1] Aston University, Birmingham B4 7ET, UK
[2] Weizmann Institute of Science, Rehovot 76100, Israel
E-mail: s.derevyanko@aston.ac.uk

New Journal of Physics **10** (2008) 075019 (16pp)
Received 21 November 2007
Published 31 July 2008
Online at http://www.njp.org/
doi:10.1088/1367-2630/10/7/075019

Abstract. We present a mean-field model of cloud evolution that describes droplet growth due to condensation and collisions and droplet loss due to fallout. The model accounts for the effects of cloud turbulence both in a large-scale turbulent mixing and in a microphysical enhancement of condensation and collisions. The model allows for an effective numerical simulation by a scheme that is conservative in water mass and keeps accurate count of the number of droplets. We first study the homogeneous situation and determine how the rain-initiation time depends on the concentration of cloud condensation nuclei (CCN) and turbulence level. We then consider clouds with an inhomogeneous concentration of CCN and evaluate how the rain initiation time and the effective optical depth vary in space and time. We argue that over-seeding even a part of a cloud by small hygroscopic nuclei, one can substantially delay the onset and increase the amount of precipitation.

[3] Author to whom any correspondence should be addressed.

Contents

1. Introduction

This paper presents an idealized model of the evolution of turbulent warm clouds with large-scale inhomogeneities in the concentration of cloud condensation nuclei (CCN). The need for such studies comes from two sets of different and urgent problems.

Firstly, the greatest uncertainty in the assessment of climate forcing by anthropogenic aerosols is their effect on clouds, referred to as the aerosol indirect effect [1]–[3]. Indirect effects of aerosols on climate is, firstly, via changes in the CCN numbers which influence the optical depth of clouds and, secondly, via precipitation rate and lifetime of clouds [4]. Since both natural and anthropogenic aerosols are often distributed very non-uniformly, it is important to develop a description of the evolution of such inhomogeneities. In particular, our study will be pertinent to stratiform clouds containing only the liquid phase, which are one of the most important in their effect on radiation (they cover 18 and 34% over land and ocean, respectively). Another possible application is to the evaluation of the global cooling geo-engineering, proposed with the use of albedo enhancement by hydroscopic seeding of maritime clouds [5, 6].

Secondly, it is often desirable to postpone rain, for instance, to bring precipitation inland from the sea [7]. Suppression of warm rain by hygroscopic seeding is also a possible mechanism of hurricane modification [8, 9]. For a recent review on cloud seeding see [10]. It is known both from observations [11]–[14] and from modelling [7] that by seeding clouds with a sufficient number of small hygroscopic aerosol particles one can delay and even suppress precipitation. This is due to a dependence of the number of activated droplets on the CCN concentration. Abundance of very small droplets at the beginning of the cloud formation may result in suppressing their collision rate and in slowing down further droplet growth. The observational data are mostly from urban pollution by large cities and natural pollution by dust storms and forest fires which seeds clouds on the scales of tens of kilometres [12]–[14]. If one desires to bring rain from the sea then seeding may be from platforms or ships, i.e. on a much smaller scales (hundreds of metres up to a kilometre). Indeed, it is known that smoke particles from ships burning fuel leave ship tracks in the clouds. Can one use cloud seeding on a sub-kilometre scale to influence precipitation? This is considered to be impractical: ‘It would be necessary to treat all portions of a target cloud because, once precipitation appeared anywhere in it, the

raindrops . . . would be circulated throughout the cloud . . . by turbulence' [15]. We believe that this conclusion ignores another, positive, aspect of cloud turbulence, namely the mixing and homogenization of partially seeded cloud during the condensation stage. Moreover, because maritime clouds appear in clean air with a small concentration of CCN, they often precipitate when a substantial amount of vapour has not condensed; we show here that seeding such clouds hygroscopically not only delays but also can substantially increase the precipitation.

Therefore, modelling a cloud with an inhomogeneous distribution of CCN is needed for checking the feasibility of hygroscopic cloud seeding, quantitatively describing effects of air pollution on precipitation, observable properties of ship-tracks in clouds etc. Another objective of this work is to develop a simple yet reliable model to account for the effects of turbulence on the distribution of droplets both over sizes and in space. Turbulence mixes horizontal and vertical inhomogeneities and enhances the collision rates. Our goal here is to quantify the interplay of these effects. Ours are 'idealized simulations, in which the interactions of physical processes are easier to discern than in the real atmosphere' [16]. In the present paper, we further develop the mean-field model introduced in [7] by accounting for the effects of turbulence.

The role of turbulence in the evolution of clouds is a subject of numerous works from (i) global circulation modelling (see e.g. [17] and the references therein) to (ii) three-dimensional (3D) large eddy simulations and observations of a given cloud (see [18]–[21] and the references therein) to (iii) micro-physical modelling of droplet condensation and collisions in a turbulent cloud, see [22]–[34]. These approaches span the scales from thousands of kilometres to microns. Our model accounts only for horizontal inhomogeneities and it is in between (i) and (ii) in scales (from one to several kilometres) while at the same time accounting phenomenologically for the microphysical effects of (iii).

2. Model

We are interested in the conditions when precipitation starts relatively fast so that clouds remain low-level and warm. We therefore consider warm clouds where droplets grow by vapour condensation on CCN and by coalescence due to collisions until the raindrops fall out of the cloud, see e.g. [4]. Those processes can be modelled by the equations for the local distribution of droplets over sizes, $n(a, \mathbf{r}, \mathbf{t})$, and the water vapour density, $M(\mathbf{r}, t)$. For simplicity, we assume that the cloud ascends in such a way that the degree of supersaturation $s = (M - M_0)/M$ stays approximately constant (here M_0 is saturated density). The equations take the form

$$\frac{\partial n}{\partial t} - \mathrm{div} D(r)\nabla n = -\frac{\kappa s M}{\rho_0}\frac{\partial}{\partial a}\frac{n(a)}{a} - n(a)\frac{u_g(a)}{L} + \int \mathrm{d}a' \left[\frac{K(a', a'')n(a')n(a'')}{2(a''/a)^2} - K(a', a)n(a')n(a)\right], \quad (1)$$

$$\frac{\partial M}{\partial t} - \mathrm{div} D(r)\nabla M = -4\pi s M \kappa \int an(a)\,\mathrm{d}a + S. \quad (2)$$

See table 1 for the definitions of the variables. The first term in the rhs of equation (1) describes condensation and is correct quantitatively up to order-unity factor [4, 7], which is enough for our purposes here. The second term there models the loss of droplets falling with the settling

Table 1. Definitions of variables.

Quantity	Units	Description
a	μm	Droplet radius
D	$\mathrm{cm^2\,s^{-1}}$	Turbulent diffusivity
$n(a)$	$\mathrm{cm^{-3}\,\mu m^{-1}}$	Distribution of droplet sizes in a unit volume
$\mathbf{r}$	km	Spatial coordinate
t	s	Time
W	$\mathrm{g\,m^{-1}}$	Amount of water in the unit volume of the cloud
T_*	s	Rain-initiation time
K	$\mathrm{cm^3\,s^{-1}}$	Collision kernel
u_g	$\mathrm{cm\,s^{-1}}$	Fall velocity
g	$\mathrm{cm\,s^{-2}}$	Acceleration of gravity
ϵ	$\mathrm{cm^2\,s^{-3}}$	Energy-dissipation rate in turbulence
ν	$\mathrm{cm^2\,s^{-1}}$	Air viscosity
ρ	$\mathrm{g\,cm^{-3}}$	Air density
ρ_0	$\mathrm{g\,cm^{-3}}$	Liquid water density
L	km	Cloud vertical size
M	$\mathrm{g\,m^{-3}}$	Water vapour density
κ	$\mathrm{cm^2\,s^{-1}}$	Water vapour diffusivity
τ	#	Optical depth of the cloud layer

velocity u_g from the cloud of the vertical size L. Since L are generally large (from tens to hundreds of metres) and $u_\mathrm{g}(a)$ grows with a, fallout is relevant only for sufficiently large drops (raindrops). Such a fallout term parametrizes conversion from cloud water to rainwater; as an alternative one can also use the usual threshold model [35]. The third term in the rhs of (1) describes coalescence due to collisions, here $a'' = (a^3 - a'^3)^{1/3}$ is the size of the droplet that produces the droplet of size a upon coalescence with the droplet of size a'. The diffusion terms in the lhs correspond to turbulent diffusivity $D(r)$ which is generally scale-dependent (see below). The last term in (2) is due to supersaturation fluctuations.

Let us stress that the model is of a mean-field nature, i.e. it is supposed to describe the quantities averaged over the vertical coordinate which thus vary at the scales comparable and exceeding the vertical extent of the cloud L. The nonlinearity of the microscopic equations (for the velocity field, temperature, vapour density and droplet distribution) does not allow a rigorous derivation of the model (by integration over the vertical coordinate and coarse-graining over the horizontal coordinates), which is thus of a semi-empirical nature and its (few) parameters must be adjusted to the results of observations. The homogeneous (r-independent) version of the model without effects of turbulence has been introduced in [7] to study the dependence of the rain-initiation time on the amount and distribution of CCN over sizes. Some analytic results for the homogeneous model are given in appendix A.

The main focus of the present work is on the effects of cloud turbulence which determines the turbulent diffusivity D and the supersaturation rate of change S and influences the collision kernel K. We characterize turbulence level by the energy-dissipation rate $\epsilon \sim 10$–$1500\,\mathrm{cm^2\,s^{-3}}$. Kolmogorov (viscous) scale is $\eta = 6\nu^{3/4}\epsilon^{-1/4}$ and the respective inverse time $\lambda = (\epsilon/\nu)^{1/2}$. We take the kinematic air viscosity $\nu = 0.15\,\mathrm{cm^2\,s^{-1}}$. For $\epsilon = 10$ one has $\lambda \simeq 8\,\mathrm{s^{-1}}$, $\eta \simeq 0.1$ cm.

We introduce also the dimensionless Stokes number characterizing inertia of the droplet of size a: $St(a) = \lambda\tau(a)$. The Stokes time is $\tau = (2/9)(\rho_0/\rho)(a^2/\nu) \approx 1.5 \times 10^3 a^2$, where a must be taken in centimetres. We neglect fluctuations in the turbulence level (i.e. the model is of a mean-field nature) and back reaction from the evolution of M and n on ϵ (briefly discussed in the summary).

2.1. Turbulent diffusion and collision rate

In the reference frame moving with the mean velocity, the character of dispersion of the spot of size r depends on r (see e.g. [36]). When r is less than the velocity correlation scale (outer scale of turbulence), Richardson super-diffusion corresponds to $D(r) = \epsilon^{1/3} r^{4/3}$. At the scales exceeding the outer scale, $D(r)$ is scale-independent. We shall always count r from the centre of the spot (of extra seeded CCN) and approximate $D(r)$ smoothly as

$$D(r) = \epsilon^{1/3}\, L^{4/3} \tanh\left[(r/H)^{4/3}\right]. \tag{3}$$

Here, we denoted the outer scale of turbulence as H which may be comparable with the height. Note that there are numerous physical situations where the diffusion approach is not enough and somewhat more regular flows participate in the spreading of the aerosol spot. Such large-scale flows can be characterized by their local velocity gradient $\mathcal{V}/\mathcal{L}$ leading to an exponential stretching of anisotropic streaks, which wins over diffusive spreading at the scales exceeding the crossover scale $\sqrt{D\mathcal{L}/\mathcal{V}}$ (see e.g. [36]). Since $D \simeq wL$ with turbulent velocity $w \simeq (\epsilon L)^{1/3}$ then the crossover scale is $\sqrt{L\mathcal{L}w/\mathcal{V}}$, i.e. for $w \simeq \mathcal{V}$ it is between L and $\mathcal{L}$. Stretching times of such regular flows are a few hours and more; here, we study inhomogeneous clouds on a shorter timescale of about an hour (see figures 5–8) so that we account for diffusion only. If necessary, it is straightforward to incorporate large-scale regular flows into our model.

The collision kernel is the product of the target area and the relative velocity of droplets on contact: $K(a, a') \simeq \pi(a + a')^2 \Delta v$. According to the recent measurements [37] the coalescence efficiency of the droplets in the relevant intervals is greater than 0.95, we put it unity in our calculations. Collisions are due to gravity fall and motion in a turbulent flow, which both contribute to the collision kernel K. We consider here relatively weak turbulence and neglect the interference between the air flow and gravity using the collision kernel as a direct sum $K = K_g + K_t$. Here, the gravity collision kernel is

$$K_g(a, a') = \pi(a + a')^2 E(a, a')|u_g(a) - u_g(a')|. \tag{4}$$

The fall velocity u_g is obtained from the balance of gravity force $4\pi g\rho_0 a^3/3$ and the drag $F(u_g, a)$. The drag force depends on the Reynolds number of the flow around the droplet, $Re_a \equiv u_g a/\nu$. When Re_a is of order unity or less, $F = 6\pi\nu\rho a u_g$ and $u_g = g\tau$ where ρ is the air density and $\tau = (2/9)(\rho_0/\rho)(a^2/\nu)$ is called Stokes time. We use $u_g = g\tau$ for $a < 40\,\mu$m and take $u_g(a)$ from the measurements [38] for $a > 50\,\mu$m with a smooth interpolation for $40\,\mu\text{m} < a < 50\,\mu$m. Hydrodynamic interaction between approaching droplets is accounted in K_g by the collision efficiency E, which values we take from [39] at the 750 mbar altitude.

According to [22]–[27], we take the turbulent collision kernel approximated as follows:

$$K_t = 4\pi\lambda a^3\{(30\pi)^{-1/2} g(a) + 0.3\exp[-1.7/St(a)]\}, \tag{5}$$

where $a = a_1 + a_2$ and $2St(a) = St(a_1) + St(a_2)$. The enhancement factor due to preferential concentration, $g(a)$, is taken as a power law: $g(a) = (\eta/a)^\alpha$ with $\alpha = (3/4)St^2/(0.1 + St^3)$ and $g(a) = 1$ when $|a_1 - a_2| > 1\ \mu$m (according to [24, 28] it works better at high Re than the linear Re dependence used in [25]).

2.2. Fluctuations of the supersaturation

Measurements in cloud cores reveal a broad size distribution of small droplets while classical air-parcel models point to narrowing size spectra during the condensation stage. As was extensively discussed before (see [4, 29, 30] and the references therein), one mechanism is the interplay between vertical inhomogeneity (of the supersaturation s) and cloud turbulence. Attempts to describe this phenomenon by introducing random vertical motion into air-parcel models [31, 32] give very limited spreading. Moreover, it has been noticed in [33] that the very notion of an air parcel is pretty much meaningless in a turbulent cloud since, for instance, two points a distance r apart separate to the viscous scale during the time $\lambda^{-1}\ln(\eta/r)$ and then to the distance R during $(R^2/\epsilon)^{1/3}$. For $\epsilon = 100\,\mathrm{cm^2\,s^{-3}}$ separating from $r = 10\,\mu$m to $R = 100\,$m takes on average less than a couple of minutes. That also means that among the droplets found in close proximity many were hundred metres apart before a minute. It has been recently demonstrated by direct numerical simulations of turbulent flows that an ability of any given droplet to span large-scale vapour fluctuations leads to a significant broadening of droplet distribution over sizes during the condensation stage [33, 34]. We assume that the vapour density has large-scale gradients (vertical due to temperature profile and horizontal due to entrainment of dry air) that can be estimated as M/L. Note that this is the estimate from below since the scales of inhomogeneities can be substantially smaller than the cloud size (hundreds and tens of metres [4, 33]). The last term in (2) is thus taken as multiplicative noise, $S = wsM/L$ (different from the additive noise wsM_0/L considered in [32]). Note that this effect is slow as it changes the vapour density on a timescale of the large-scale turnover time. Indeed, the inverse turnover time, $w/L \simeq (\epsilon/L^2)^{1/3} \leqslant 10^{-3}\,\mathrm{s^{-1}}$, is generally much smaller than both the inverse droplet growth time, $\kappa M/\rho_0 a^2 \simeq 10^{-2}\,\mathrm{s^{-1}}$, and the vapour depletion rate, $4\pi\kappa an \sim 12 \times 0.25\,\mathrm{cm^2\,s^{-1}} \times 50\,\mathrm{cm^{-3}} \times 10^{-3}\,\mathrm{cm} \simeq 0.15\,\mathrm{s^{-1}}$. However, we shall show that it may lead to significant changes because even a small broadening of droplet distribution over sizes dramatically increases gravitational collisions. We assume that during the (relatively short) condensation stage clouds ascend in such a way that the supersaturation s stays approximately constant. In a future sophistication of the model, one can consider temperature T (related to cloud height) as an independent variable and treat supersaturation as a function $s(T)$. That will allow to account for convection and other phenomena.

The homogeneous system

$$\frac{\partial n}{\partial t} = -\frac{\kappa s M}{\rho_0}\frac{\partial}{\partial a}\frac{n}{a} - \frac{u_g n}{L} + \int \mathrm{d}a' \left[\frac{K(a', a'')n(a')n(a'')}{2(a''/a)^2} - K(a', a)n(a')n(a)\right], \tag{6}$$

$$\frac{\mathrm{d}M}{\mathrm{d}t} = -4\pi M\kappa s \int an(a)\mathrm{d}a + \frac{wsM}{L}, \tag{7}$$

allows one to study the role of supersaturation fluctuations in broadening the distribution over sizes and accelerating rain. Here, we take $w(t)$ as a short correlated process with the variance $\langle w^2\rangle = (\epsilon R)^{2/3}$, where R is the smallest among L and the collision mean free path $r_c = (4\pi E \int n(a)a^2\mathrm{d}a)^{-1}$.

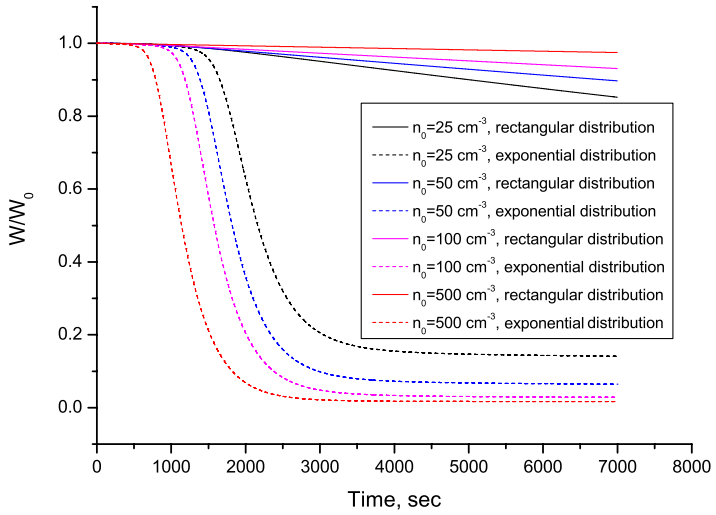

Figure 1. Fraction of water left in the cloud as a function of time, $\epsilon = 0$.

The fluctuations of supersaturation are particularly important at the early stage when condensation dominates the droplet growth and collisions and fallout can be neglected. The system then takes the form

$$\frac{\mathrm{d}a^2}{\mathrm{d}t} = -\frac{2\kappa s M}{\rho_0}, \tag{8}$$

$$\frac{\mathrm{d}M}{\mathrm{d}t} = -4\pi M \kappa s \int an(a)\mathrm{d}a + \frac{wsM}{L}. \tag{9}$$

3. Rain-initiation time in a homogeneous case

Here, we show how the rain-initiation time T depends on different parameters. We solve numerically the homogeneous system (6), (7) with $M(0) = M_0 = 1\,\mathrm{g\,m^{-3}}$ and $s = 0.01$. We use the numerical scheme first suggested in [7] (see appendix B). Without turbulence ($\epsilon = 0$), as expected, timescales of precipitation depend dramatically on the form of initial distribution as seen from figure 1 that shows the total water density $W(t) = M(t) + (4\pi\rho_0/3)\int n(a,t)a^3\,\mathrm{d}a$ normalized to its initial value W_0. For a rectangular initial distribution within the interval 1–3 μm, precipitation develops very slowly due to condensation–collision bottleneck. On the other hand, the initial distribution with an exponentially decaying tail towards large sizes (which models the presence of a small number of so-called ultra-giant nuclei), $n(a,0) = (n_0/3)\exp(-(a-1)/3)$, where a is measured in micrometres ($a > 1$), provides for a dramatic acceleration of droplet growth and fallout in agreement with [40, 41]. The figure also shows that too small CCN number leads to substantial residual water remaining in the cloud after a rainfall. Taking clouds with a small number of CCN (less than $100\,\mathrm{cm^{-3}}$) and seeding them may thus lead to a substantial increase of precipitation (up to 15% according to figure 1).

Following [7], we define the rain-initiation time, T_*, as the point where the absolute value of the second derivative $|\mathrm{d}^2W(t)/\mathrm{d}t^2|$ is maximal (another possible choice is the inflection point in the dependence $W(t)$ which gives practically the same results). Figure 2(a) corresponds to the system (6), (7) without the last term (which accounts for supersaturation fluctuations), it shows that already an account of turbulence enhancement of collisions substantially accelerates droplet

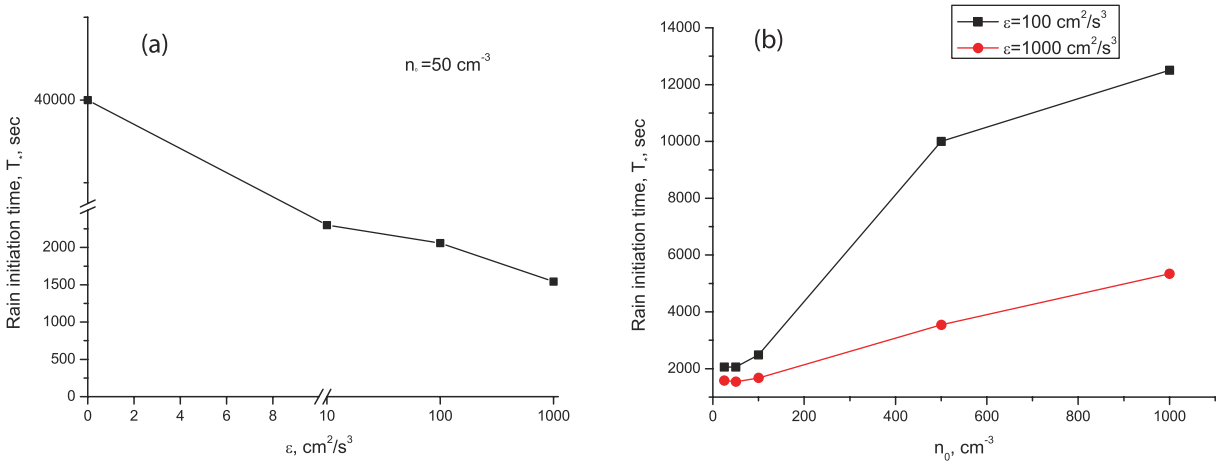

Figure 2. Rain-initiation time versus turbulence level (a) and versus the CCN number (b). $M_0 = 1\,\mathrm{g\,m^{-3}}$, rectangular initial distribution 1–3 μm.

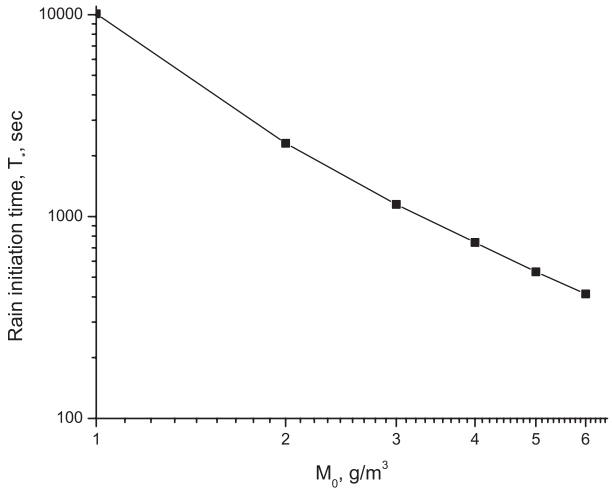

Figure 3. Rain-initiation time versus the initial vapour density for $n_0 = 500\,\mathrm{cm^{-3}}$, $\epsilon = 100\,\mathrm{cm^2\,s^{-3}}$, rectangular initial distribution 1–3 μm.

growth and fallout. Under the same condition, we obtain the data presented in figure 2(b), which are of most interest for what follows. These data quantify the growth of the rain-initiation time with the CCN number (when it is sufficiently large—the whole non-monotonic dependence has been obtained within a more crude model without turbulence [7]). Note that when T_* is getting large enough clouds may come into an environment where they evaporate, so that seeding can indeed be not only a mechanism of rain delay but also of rain suppression [42]. In the next section, we shall exploit the growth of T_* with n_0 to show that one can locally over-seed a cloud front to get a substantial effect of rain delay in a wide area.

Figure 3 shows the dependence of the rain-initiation time on the initial water vapour density M_0. We see that $T_*(M_0) \simeq M_0^{-c}$ with c between 1.7 and 1.8. Since the condensation time decays as $M_0^{-1/3}$, i.e. much slower, it is clear that in this regime the rain initiation time is determined by collisions. According to the predictions of [7], $T_* \propto M_0^{-\alpha/3}$ at not very high M_0, assuming

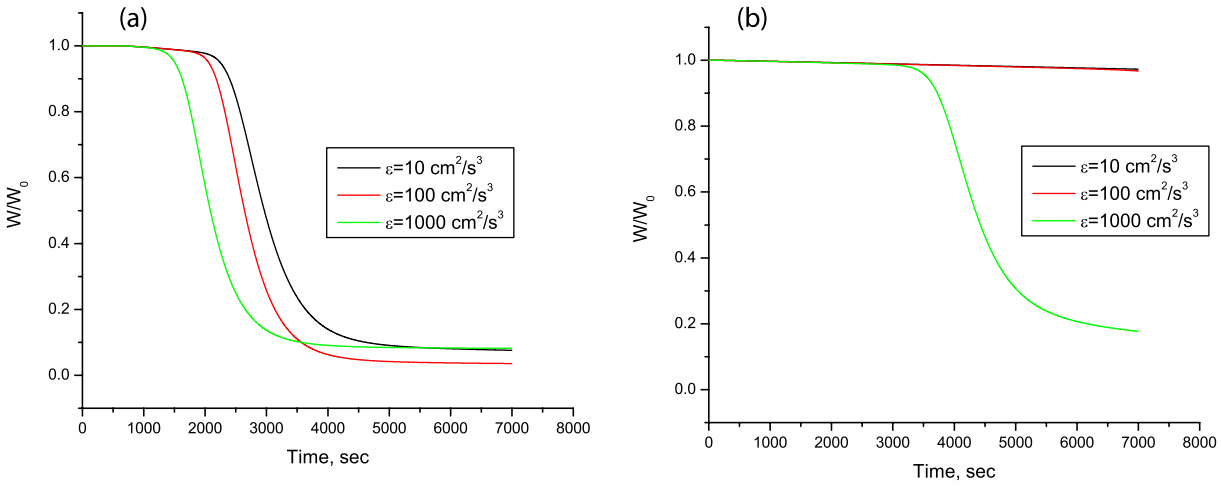

Figure 4. Fraction of water left in the cloud as a function of time with the account of supersaturation fluctuations. $M_0 = 1\,\mathrm{g\,m^{-3}}$. (a) $n_0 = 50\,\mathrm{cm^{-3}}$ and (b) $n_0 = 500\,\mathrm{cm^{-3}}$.

that the collision kernel behaves as a power law: $K \propto a^{\alpha}$. Figure 3 thus suggests an effective α between 5.4 and 5.6.

Let us now add an effect of supersaturation fluctuations. The simulation comprises three stages. During the first stage a truncated system (8), (9) is simulated and we determine the average time $\langle T \rangle$ for which the vapour content M falls below the threshold of 30% of its initial value. The average is computed from 5000 Monte Carlo runs. Then another Monte Carlo simulation is performed of the same system (8), (9) when the evolution of the fluctuating distribution $n(a, t)$ and $M(t)$ are followed up to the time $t = \langle T \rangle$ when the average size distribution $\langle n(a, \langle T \rangle) \rangle$ and $\langle M(\langle T \rangle) \rangle$ are determined in such a way that the total amount of water, W, is conserved. Afterwards the averaged size distribution and vapour density are inserted as initial conditions for the system (6), (7) but this time the fluctuating term in (7) is neglected since vapour is already depleted. Figure 4 presents the results obtained within the framework of (6), (7).

We see that an account of supersaturation fluctuations in the framework of our multiplicative noise model does not significantly change the timescales yet affects the amount of residual water (which depends non-monotonically on the turbulence level as seen in figure 4(a)).

We conclude this section by remarking that acceleration of the rain initiation by turbulence (in either condensation or collision stage) is comparable to that by ultra-giant nuclei in the interval of parameters studied.

4. Evolution of clouds with non-uniform CCN distribution

Here, we consider cloud evolution under the action of an external source of CCN localized in space. In this case, both n and M depend on the spatial coordinate r. Turbulent diffusion provides for an exchange between different regions marked by different r. Depending on the space dimensionality d, the radial part of the diffusion operator takes the following form: $\mathrm{div} D(r) \nabla = r^{1-d} \partial_r r^{d-1} D(r) \partial_r$.

Our model is averaged over the vertical coordinate so it is applied only to horizontal large-scale mixing. That means that it is supposed to work on a timescale exceeding the time $(L^2/\epsilon)^{1/3}$ needed for vertical homogenization.

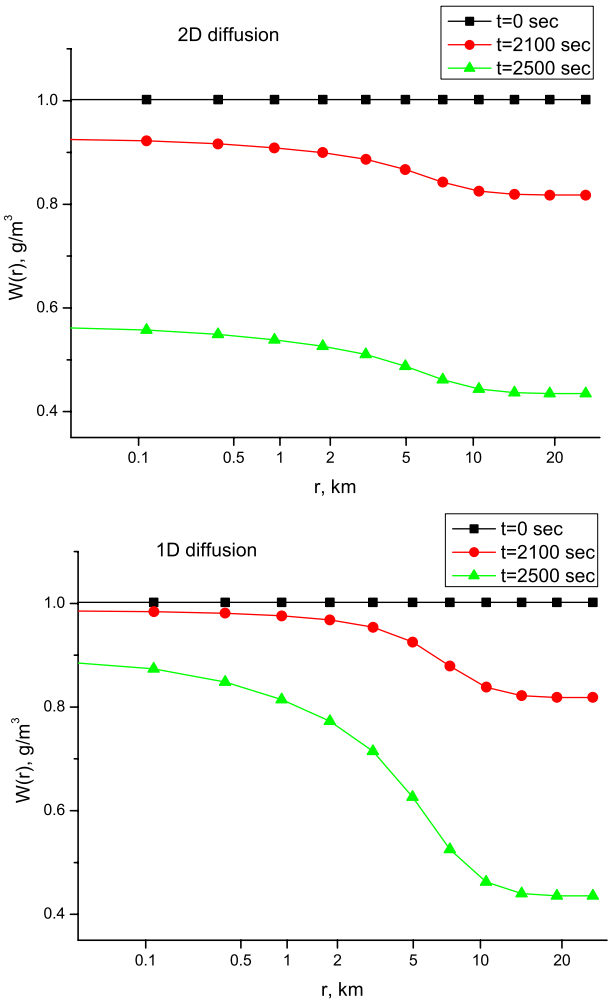

Figure 5. Spatial distribution of the fraction of water left in the cloud for three different times. Top panel 2d, seeding of a circular spot, r is the radial coordinate. Bottom panel 1d, seeding a strip, r is the coordinate across the strip.

We start from a 2d axially symmetric case, i.e. we consider a circular spot of additional CCN released at the beginning ($t = 0$). The initial distributions over sizes in all cases were rectangular between 1 and 3 μm multiplied by the distribution in space $n_0 + n_1 \exp(-r^2/2l^2)$ with the values $l = 1$ km, $n_0 = 50\,\mathrm{cm}^{-3}$ and $n_1 = 1000\,\mathrm{cm}^{-3}$. We take the initial distribution of vapour $M(r, 0) = M_0 - M_1 \exp(-r^2/2l^2)$ with $M_0 = 1\,\mathrm{g\,m}^{-3}$ and $M_1 \approx 0.04\,\mathrm{g\,m}^{-3}$ so that $W(r, 0)$ was uniform at $t = 0$. We take $H = 500$ m, $L = 2$ km and $\epsilon = 100\,\mathrm{cm}^2\,\mathrm{s}^{-3}$. Some details of the numerical scheme are given in appendix B. Figure 5 shows $W(r, t)$, i.e. the amount of water in grams per cubic metre left in the cloud as a function of space and time. One can see how turbulence spreads the seeding and how precipitation is delayed in a widening region. The increase in the amount of water left in the cloud is given by $2\pi L \int_0^R [W(r, t) - W(R, t)]r\,\mathrm{d}r \simeq 1.7 \times 10^7$ kg after $t = 2500$ s for seeding by $n_1 \times L \times \pi l^2 \simeq 6 \times 10^{18}$ CCN particles. Here, $R = 25$ km is the radius of the simulation domain.

Let us now describe how seeding influences optical properties of the cloud characterized by the optical depth which is determined by the effective droplet area and the cloud height:

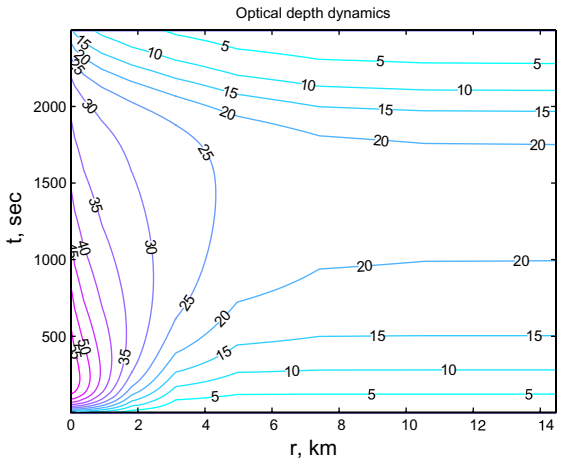

Figure 6. Spatio-temporal isolines of optical depth for seeding a circular spot of radius 1000 m at $t = 0$ by an extra $n_1 = 1000\,\mathrm{cm}^{-3}$.

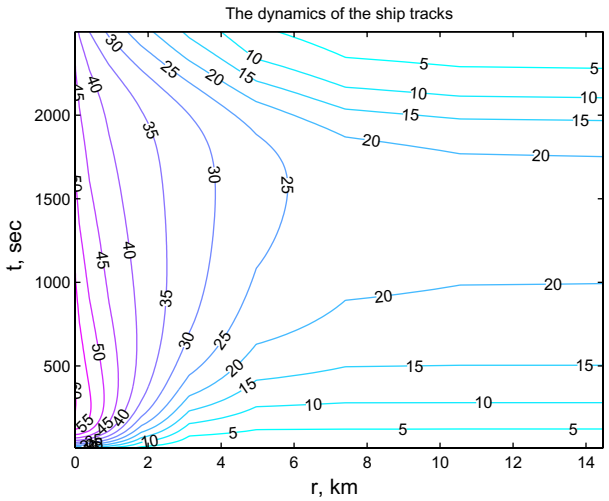

Figure 7. The spreading of a ship track for $\varepsilon = 10\,\mathrm{cm}^2\,\mathrm{s}^{-3}$. Initial spot size was 1 km and $n_1 = 1000\,\mathrm{cm}^{-3}$ particles were seeded.

$\tau(r,t) = \pi L \int a^2 n(a,r,t)\mathrm{d}a$. For drops larger than the wavelengths of visible light, albedo is equal to $\tau/(\tau+7.7)$ [4]. Figure 6 shows the plot of $\tau(r,t)$ for the same initial distribution and $\epsilon = 10\,\mathrm{cm}^2\,\mathrm{s}^{-3}$ (more appropriate for stratus clouds).

Consider now a 1d situation, $d = 1$. It corresponds either to an initial seeding along a strip or to a stationary situation when clouds move relative to the permanently acting seeding source. For a stationary situation, t is to be interpreted as a spatial coordinate (divided by the cloud speed with respect to the source). This is particularly similar to ship tracks which can be seen in marine stratus clouds as cloud reflectivity changes in the wake of the exhaust of a ship's engine. Figure 7 shows how a track from a moving source looks in our model (again, t must be multiplied by the source speed to give a distance from the source). Another situation we have in mind is a cloud front moving with respect to a stationary permanently acting source

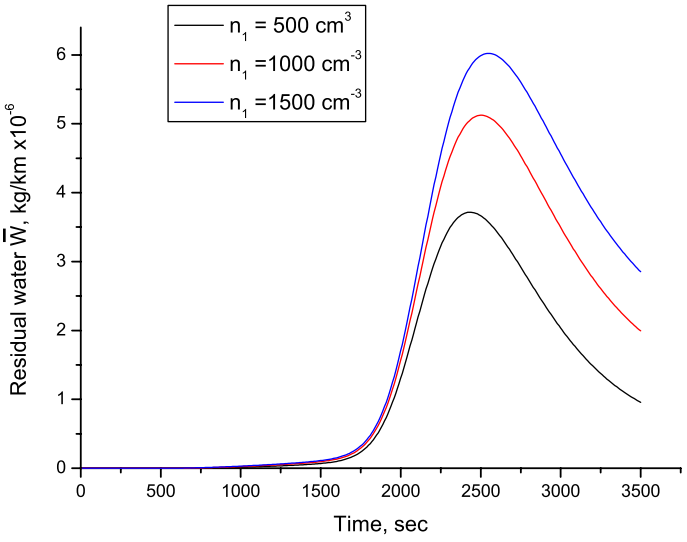

Figure 8. The difference, $\bar{W}$, in the total amount of water left in the cloud (per unit distance from the shoreline) due to seeding.

of CCN intended to postpone precipitation. This is particularly important in cases (like Israel, California, etc) where rains are in winter when the sea is warmer than the shore. As a result, clouds coming from the sea start raining before coming ashore. Let us see how much water one can move further downwind by a local permanent seeding in our model. Bottom panel of figure 5 shows the distribution of water left in the cloud. Comparison of the top and bottom panels, unsurprisingly confirms that continuous seeding is much more effective than releasing a puff. Figure 8 shows how much one can increase the amount of water left in the cloud front (per unit distance from the coastline) $\bar{W}(t) = L\int_0^R [W(r,t) - W(R,t)]\,\mathrm{d}r$ by seeding with different amounts of CCN. To put that into numbers we take wind speed $u = 10\,\mathrm{m\,s^{-1}}$ and see that by seeding $n_1 \times L \times l \times u = 10^{16}$ particles per second (the weight of smoke micro-particles that can serve as CCN is 10^{-15}–10^{-14} g), we get the increase of cloud-carried water flux $\bar{W}(t) \times u \simeq 10^4\,\mathrm{kg\,s^{-1}}$ across the shoreline at the distance $ut = 20\,\mathrm{km}$ from the source of seeding.

5. Summary

We have presented a model of cloud evolution that incorporates both macroscopic and microscopic effects of turbulence. This model should be considered as but a first crude attempt to put together the results of numerous studies of different groups to consistently incorporate turbulence effects on all scales into the description of warm clouds. Practically every aspect, from micro-scale effects (condensation and collisions) to macro-scale mixing needs further elaboration. In particular, spectrum broadening during the condensation stage deserves more detailed studies. Inhomogeneous seeding provides for inhomogeneous heat release rate due to condensation and provides for inhomogeneous turbulence which enhances the mixing, we believe that can be incorporated into our model by making ϵ dependent on the condensation rate. Generally, it is pretty straightforward to incorporate into this model an extra equation

relating ϵ change to M and n. Such feedback relations are to be established from detailed studies of 3d local structure of clouds and turbulence by large eddy simulations and other methods (see [19]–[21] and the references therein). The feedback mechanisms and relations may be different for different types of clouds; much future work is needed here. Next, suppression of low-level rainout and aerosol washout allows transport of water to upper levels where it can freeze so that a consistent description must take ice into account as well.

Still, within the timescales and parameters considered the model gives answers with a reasonable order of magnitude. To fine-tune the parameters, comparison with the observations that include the same set of variables is needed, it requires further work. After such fine-tuning, the model can be useful not only in extracting qualitative dependences between parameters but also in obtaining quantitative estimates. We believe that calculations within the framework of such mean-field models can present parametrization schemes to be used for cloud description (particularly for an account of inhomogeneous CCN concentration) in mesoscale models.

Let us now answer the question on rain delay by over-seeding posed in the introduction. Based on the present results we can conclude that well before the seeded area is 'infected' by raindrops from outside it is spread in space to the extent that makes such an over-seeding a practical possibility. We believe that this line of study is worth pursuing further.

Acknowledgments

The work has been supported by the grants of the EPSRC, Minerva and the Israeli Science Foundations and by the Minerva Einstein Center funded through the BMBF.

Appendix A. Condensation with fallout

During the initial stage, when collisions and the fluctuations of the supersaturation can be neglected and $u_g = \alpha a^2$ (Stokes law), the spatially uniform equation

$$\frac{\partial n}{\partial t} = -\frac{\kappa s M}{\rho_0}\frac{\partial}{\partial a}\frac{n(a)}{a} - n(a)\frac{u_g(a)}{L}$$

has an analytic solution for $f(a^2, t) = n(a, t)/a$ determined by the initial condition $f(a^2, 0) = f_0(a^2)$:

$$f(a^2, t) = f_0(a^2 - \beta(t)) \exp\left[\frac{\alpha}{L}\left(\int_0^t \dot{\beta}(t')\, t'\, \mathrm{d}t' - a^2 t\right)\right],$$

$$\beta(t) = (2\kappa s/\rho_0) \int_0^t M(t')\mathrm{d}t'. \tag{A.1}$$

From (7) (without the fluctuating term) and (A.1) one obtains an integral equation for M that can be solved by iterations:

$$M(t) = M(0) \exp\left\{-2\pi\kappa s \int_0^t \mathrm{d}z \exp\left[-\frac{\alpha}{L}\frac{2\kappa s}{\rho_0}\int_0^z M(u)(z-u)\mathrm{d}u\right]\right.$$
$$\left. \times \int f_0(a^2)(a^2 + \beta(t))^{1/2} \exp[-\alpha z a^2/L]\mathrm{d}\,(a^2)\right\}. \tag{A.2}$$

It is useful to introduce normalized units: $T = t/\tau$, $x = (a/\bar{a})^2$, $\tilde{f}(x) = f(x)\,\bar{a}^2/n_0$, $m(T) = M(t)/M(0) = M(t)/M_0$, here $\bar{a} = (3M_0/(4\pi\rho_0 n_0))^{1/3}$, $n_0 = \int n(a,a)\mathrm{d}a$, $\tau = (4\pi\kappa s n_0 \bar{a})^{-1}$ and the dimensionless parameter

$$\tilde{\epsilon} = \frac{\alpha\,\tau\,\bar{a}^2}{L} = \frac{\alpha\bar{a}}{4\pi\,\kappa s\,L\,n_0} \propto n_0^{-4/3}.$$

Then, the equation for m can be written as

$$m(T) = \exp\left\{-(1/2)\int_0^T \mathrm{d}z \exp\left[(2\tilde{\epsilon}/3)\int_0^z m(u)(z-u)\mathrm{d}u\right]\right.$$
$$\left.\times \int_0^\infty \tilde{f}_0(x)\left(x + (2/3)\int_0^T m(p)\mathrm{d}p\right)^{1/2} \exp[-\tilde{\epsilon}\,z\,x]\mathrm{d}x\right\}. \tag{A.3}$$

Let us make some numerical estimates. Let us take $M_0 = 1\,\mathrm{g\,cm^{-3}}$, $n_0 = 50\,\mathrm{cm^{-3}}$, $L = 2\,\mathrm{km}$, $s = 0.01$, $\kappa = 0.25\,\mathrm{cm^2\,s^{-1}}$ and finally $\alpha = (2/9)\,(g/\nu)\,(\rho_0/\rho) = 1.5\times 10^6\,\mathrm{cm^{-1}\,s^{-1}}$. This yields $\bar{a} \approx 17\,\mu\mathrm{m}$, $\tau \approx 378\,\mathrm{s}$ and $\tilde{\epsilon} \approx 8$. The latter estimate shows that the effects of gravitational fallout cannot be neglected when the water is depleted.

Appendix B. The numerical scheme

Equations (1) and (2) can be rewritten in a formal operator form:

$$\frac{\partial}{\partial t}\begin{pmatrix} n(a,r,t) \\ M(r,t)\end{pmatrix} = (\hat{\mathcal{D}}_\epsilon + \hat{\mathcal{K}})\begin{pmatrix} n(a,r,t) \\ M(r,t)\end{pmatrix}, \tag{B.1}$$

where $\hat{\mathcal{D}}_\epsilon = r^{-1}\,\partial_r\,\epsilon^{1/3}\,r^{7/3}\,\partial_r$ is the operator of turbulent diffusion and $\hat{\mathcal{K}}$ encompasses the collision term in (1) as well as the effects of sedimentation and vapour condensation. Note that operators $\hat{\mathcal{D}}_\epsilon$ and $\hat{\mathcal{K}}$ act upon different variables: the former describes propagation in space while the latter forms the size distribution locally at each point in space. Since the two operators have physically different origins we use the *split-operator* technique to propagate the solution. Indeed using the Baker–Hausdorff formula, we can write an infinitesemal propagator of the distribution $n(r,a,t)$ as

$$n(r,a,t+\Delta t) = \exp[(\hat{\mathcal{D}}_\epsilon + \hat{\mathcal{K}})\,\Delta t]\,n(r,a,t)$$
$$= \exp[\hat{\mathcal{D}}_\epsilon\,\Delta t]\,\exp[\hat{\mathcal{K}}\,\Delta t]\,\exp\left[-\tfrac{1}{2}[\hat{\mathcal{D}}_\epsilon, \hat{\mathcal{K}}]\,\Delta t^2 + O(\Delta t^3)\right]. \tag{B.2}$$

If we neglect the non-commutating nature of operators $\hat{\mathcal{D}}_\epsilon$ and $\hat{\mathcal{K}}$, that is we neglect the last factor in (B.2), we will have the scheme that is first-order in Δt. The accuracy can be readily increased if we use a symmetrized split-operator scheme:

$$n(r,a,t+\Delta t) = \exp[\hat{\mathcal{D}}_\epsilon\,\Delta t/2]\,\exp[\hat{\mathcal{K}}\,\Delta t]\,\exp[\hat{\mathcal{D}}_\epsilon\,\Delta t/2]. \tag{B.3}$$

From the Baker–Hausdorff formula it follows that scheme (B.3) is, in fact, a second-order scheme in Δt.

We use the following schemes for the individual propagators $\exp[\hat{\mathcal{D}}_\epsilon\,\Delta t/2]$ and $\exp[\hat{\mathcal{K}}\,\Delta t]$. First of all, we note that $\exp[\hat{\mathcal{D}}_\epsilon\,\Delta t/2]$ is the subdiffusive heat kernel and its coordinate representation $G(r,r',t)$ (Green function) is well known [36]. It has a sub-Gaussian asymptote at large distance, R, from the origin $G(R,0,t) \propto \exp[-\mathrm{const}\,R^{2/3}/(\epsilon^{1/3}t)]$. In the numerical

simulation it is convenient to make a variable substitution $x = r^{1/3}$. In this new variable the diffusive behaviour is close to normal diffusion and we can use standard numerical schemes for the diffusion operator. In our simulation, we used an implicit scheme in discrete time variable t_i. A standard von Neumann analysis yields the following stability criteria:

$$\alpha \equiv \frac{\epsilon^{1/3}\,\Delta t}{(\Delta x)^2} < \frac{1}{2(d-1/3)^2}, \tag{B.4}$$

where Δt is the fixed time step, Δx is the fixed step in the variable x, and $d = 1$ and 2 is the dimensionality of the problem. In our simulations, the computational boundary was $R_* = 25$ km and the number of discrete coordinate points N_x was 12. This insures that stability criterion (B.4) is fulfilled while the number of points falling inside of the initial distribution peak is estimated as $N_l = N_x\,(l/R_*)^{1/3} \approx 3$ which is enough for our purposes.

As for the size distribution propagator $\exp[\hat{\mathcal{K}}\,\Delta t]$, we will use the highly efficient scheme which was first suggested in [7]. In this scheme, the droplet radii are discretized so that at each point r the distribution is presented as the set of concentrations $n_i(r, t)$ of droplets with radii between a_i and $a_i + \Delta a_i$. In our simulations, the grid was taken to be exponential with 512 points ranged between $a_{\min} = 1\ \mu$m and $a_{\max} = 10^4\ \mu$m. The collision term in (1) is treated as follows: let the radius $(a_i + a_j)^{1/3}$ of the droplet resulting from the merging of two droplets with radii a_i and a_j be in between the two radii a_k and a_{k+1} from the grid. Then the collision results in decreasing n_i and n_j by the quantity $\Delta N = K(a_i, a_j)n_i n_j \Delta t$, while the concentrations n_k and n_{k+1} are increased in such a way that the sum of their change is ΔN and the whole amount of water in droplets is conserved in coalescence:

$$\delta n_i = \delta n_j = -\Delta N = -\delta n_k - \delta n_{k+1},$$
$$a_k^3 \delta n_k + a_{k+1}^3 \delta n_{k+1} = (a_i^3 + a_j^3)\Delta N.$$

From these two equations follow the sought increments:

$$\begin{aligned} \delta n_{k+1} &= \Delta N(a_i^3 + a_j^3 - a_k^3)/(a_{k+1}^3 - a_k^3), \\ \delta n_k &= \Delta N(a_{k+1}^3 - a_j^3 - a_i^3)/(a_{k+1}^3 - a_k^3). \end{aligned} \tag{B.5}$$

If ΔN is greater than either n_i or n_j, we choose $\Delta N = \min(n_i, n_j)$ to keep the numbers positive.

The condensation term in (1) was treated separately using an explicit finite differencing scheme which was adjusted to conserve the total amount of water $W(t)$. The treatment of the sedimentation term in (1) and the condensation term in the rhs of (2) does not present any difficulties.

References

[1] Twomey S A 1977 *J. Atmos. Sci.* **34** 1149–52
[2] Cotton W R and Pielke R A 1995 *Human Impacts on Weather and Climate* (New York: Cambridge University Press)
[3] Pilewskie P 2007 *Nature* **448** 541–2
[4] Pruppacher H R and Klett J D 1997 *Microphysics of Clouds and Precipitation* (Dordrecht: Kluwer)
[5] Latham J 2007 *Nature* **347** 339–40
[6] Morton O 2007 *Nature* **447** 132–6
[7] Falkovich G, Stepanov M and Vucelja M 2006 *J. Appl. Meterol. Climate* **45** 591–9
[8] Rosenfeld D, Khain A, Lynn B and Woodley W L 2007 *Atmos. Chem. Phys.* **7** 3411–24

[9] Cotton W R, Zhang H, McFarquhar G M and Saleeby S M 2007 *J. Weather Modification* **39** 70–3
[10] Bruintjes R T 1999 *Bull. Am. Meterol. Soc.* **80** 805–20
[11] Gunn R and Phillips B B 1957 *J. Meteorol.* **14** 272
[12] Warner J 1968 *J. Appl. Meteorol.* **7** 247–51
[13] Rosenfeld D 2000 *Science* **287** 1793
[14] Andreae M O *et al* 2004 *Science* **303** 1337
[15] Dennis A S 1980 *Weather Modification by Cloud Seeding* (New York: Academic)
[16] Randall D, Khairoutdinov M, Arakawa A and Grabowski W 2003 *Bull. Am. Meterol. Soc.* **85** 1547
[17] Schmidt G A *et al* 2006 *J. Climate* **19** 153–92
[18] Nicholls S 1984 *Q. J. R. Meterol. Soc.* **110** 783–820
[19] Stevens B *et al* 2005 *Mon. Weather Rev.* **133** 1443–62
[20] Kogan Y L 2006 *J. Atmos. Sci.* **63** 952–67
[21] Abel S J and Shipway B J 2007 *Q. J. R. Meteorol. Soc.* **133** 781–94
[22] Falkovich G, Fouxon A and Stepanov M G 2002 *Nature* **419** 151–4
[23] Franklin C, Vaillancourt P, Yau M K and Bartello P 2005 *J. Atmos. Sci.* **62** 2451–66
[24] Falkovich G and Pumir A 2004 *Phys. Fluids* **16** L47–50
Falkovich G and Pumir A 2007 *J. Atmos. Sci.* **64** 4497–505
[25] Riemer N and Wexler A S 2005 *J. Atmos. Sci.* **62** 1962–75
[26] Chun J, Koch D L, Rani S L, Ahluwalia A and Collins L 2005 *J. Fluid Mech.* **536** 219–51
[27] Derevyanko S, Falkovich G, Turitsyn K and Turitsyn S 2007 *J. Turbulence* **8** 1–18
[28] Sundaram S and Collins L 1997 *J. Fluid Mech.* **335** 75–109
[29] Korolev A 1995 *J. Atmos. Sci.* **52** 3620–34
[30] Shaw R 2003 *Annu. Rev. Fluid Mech.* **35** 183–227
[31] Vaillancourt P A, Yau M K, Bartello P and Grabowski W W 2002 *J. Atmos. Sci.* **59** 3421–35
[32] Turitsyn K 2003 *Phys. Rev.* E **67** 062102
[33] Celani A, Falkovich G, Mazzino A and Seminara A 2005 *Europhys. Lett.* **70** 775–81
[34] Celani A, Mazzino A, Seminara A and Tizzi M 2007 *J. Turbulence* **8** 1–9
[35] Kessler E 1969 *Meteorology Monograph No 32* (Boston: American Meteorological Society)
[36] Falkovich G, Gawedzki K and Vergassola M 2001 *Rev. Mod. Phys.* **73** 913
[37] Beard K V, Durkee R I and Ochs H T 2002 *J. Atmos. Sci.* **59** 233–43
[38] Gunn R and Kinzer G D 1949 *J. Meteorol.* **6** 243
[39] Pinsky M, Khain A and Shapiro M 2001 *J. Atmos. Sci.* **58** 742–66
[40] Johnson D B 1982 *J. Atmos. Sci.* **39** 448–60
[41] Levin Z, Wurzler S and Reisin T 2000 *J. Geophys. Res.* **105** 4501–12
[42] Rosenfeld D and Gutman G 1994 *Atmos. Res.* **34** 259–83